ACCEPTED MANUSCRIPT

Published version available at:

https://doi.org/10.1016/j.combustflame.2020.11.026

-

Flame-acoustics interaction for symmetric and non-symmetric flames propagating in a narrow duct from an open to a closed end.

Carmen Jiménez, Daniel Fernández-Galisteo and Vadim N. Kurdyumov

Energy Department, CIEMAT, Avda. Complutense, 40, 28040 Madrid, Spain
http://rdgroups.ciemat.es/web/grupocombustion/inicio
carmen.jimenez@ciemat.es

Abstract

We present a numerical study of the interaction of the flame and acoustic waves when a laminar flame propagates in a narrow channel from an open to a closed end. It is shown that the coupling of the flame dynamics and the acoustics can lead to thermo-acoustic instabilities, that can result in large oscillations in the flame speed and pressure inside the duct. Additionally, it is shown that both symmetric and non-symmetric flames can propagate in these channels and that, because their response to acoustic oscillations is different, their interaction with the acoustic modes of the channel is also different. Therefore, the possibility of symmetry breaking needs to be taken into account in order to correctly predict the onset of acoustic flame instabilities in narrow channels.

Keywords:
micro combustion; flame instabilities; thermo-acoustic instabillities; flames in narrow channels; non-symmetric flames

1. Introduction

Small-scale combustion has received a lot of interest recently as a power and heat generation technology, because of potential advantages compared to existing small-scale batteries, such as lower weight, smaller size, higher power output, faster recharge and longer duration. Reviews of recent technologies and developments can be found in [1–6].

Obtaining high power in small-scale combustion systems requires completion of the combustion process in a small volume and is then limited by the chemical reaction time characteristics of the fuel. Moreover, the increased surface-to-volume ratio of small devices results in large heat losses through the wall, which can affect the stability of the flame. As a consequence, the coupling between the fluid dynamics, heat transfer, acoustics and chemical kinetics is important in these small systems and is a critical element of their design.

The propagation of flames in ducts (small or large) is also of interest for safety reasons: when a mixture of fuel and oxidizer can exist in the injection conducts of a combustion system, it is fundamental to know if a flame can propagate upstream along them, a situation known as flashback. After pioneering work in this subject about thirty years ago [7, 8], recent interest in small-scale combustion systems has motivated further studies on the effects of heat losses, the flow velocity, the Lewis number and the channel width on the flame propagation and extinction limits for steady flames propagating in narrow channels [9–19]. In these works, the extraordinary complexity of the flame dynamics has been evidenced. In particular it was shown that several flame instabilities can appear, related to heat expansion, to differential diffusion or to the effect of varying viscosity.

Nevertheless, studies of flame-acoustics interactions leading to acoustic instabilities for flames in small ducts are scarce in literature. Until recently, experiments on thermo-acoustic instabilities have only been viable in meso-scale ducts (diameters of the order of $1-10$ cm) [20–23]. They have shown that when a flame propagates from an open to a closed end in a conduct the coupling of flame dynamics and pressure can lead to different regimes: for mixtures for which the flame propagation speed is slow the flame produces no sound; for more energetic mixtures a primary instability is detected, in which the flame oscillates moderately while propagating and sound is produced; when the laminar flame speed of the mixture is large, violent acoustic instabilities (called secondary), featuring large flame oscillations and high intensity sound are reported and finally for even faster flames, the interaction flame-acoustics leads to incoherent, very fast motion and the flame becomes turbulent, producing no sound [21]. Experimental studies of flame-acoustics interactions in smaller systems have only been reported recently, in a series of studies of different fuel flames propagating towards a closed end in the narrow gap between two parallel plates (a Hele-Shaw cell), showing again primary and secondary thermo-acoustic instabilities [24, 25]. In these experiments the narrower dimension was of the order of 1-10 mm.

Analytical and numerical studies of flame-acoustics interactions have usually decoupled the acoustic problem from that of the flame, to simplify the problem and facilitate the analysis and have studied the response of planar or slightly wrinkled flames to forcing by externally imposed acoustic waves [26–28]. To the best of our knowledge, the two-way coupling between flame and acoustics in a conduct using direct numerical simulations of the complete problem has only been tackled in the study reported by Petchenko et al. [29, 30]. In these two papers, numerical simulations solving the flame propagation and the acoustics for flames propagating in narrow channels with adiabatic walls and $Le = 1$ were presented. However, the possibility of symmetric and non-symmetric propagating flame solutions was overlooked.

Several recent studies have indeed shown that in narrow channels symmetric and non-symmetric flame solutions might appear, related to thermo-diffusive or Darrieus-Landau instabilities [12, 13, 17, 19, 31]. This symmetry breaking in otherwise perfectly symmetric problems appears at a critical channel width, which depends on the reactants flow rate, the mixture Lewis number and the heat release parameter. When symmetry breaking occurs and the two solutions are mathematically possible, symmetric flames have been shown to be unstable to small perturbations, and non-symmetric flames emerge as the physically realizable solutions. For a given set of parameters, the non-symmetric slanted-shaped solution presents a significantly larger flame surface and propagating speed than the corresponding symmetric flame. Because these differences can be relevant for the flame-acoustics interactions, here we revisit the above mentioned study [29, 30], paying special attention to the possibility of symmetry breaking and its implications in the onset of thermo-acoustic instabilities.

Notice that in [25–28], where flames in vertical channels were investigated, it was concluded that gravitational acceleration plays an important role in the flame instability. Nevertheless, we shall neglect gravity forces in this work, and will study their effect elsewhere. In addition, we will simplify the problem studying only $Le = 1$ flames in adiabatic channels, and will include differential diffusion and heat losses to the walls in future work. The main goal of this work is to study the effect of flame symmetry on the dynamics of flame-acoustic interaction.

In section 2 we describe briefly the adopted set-up, the conservation equations and the numerical method used to solve them; in section 3 we present flames propagating in a narrow adiabatic channel with a closed end and the conditions for the existence of symmetric and non-symmetric solutions, which for a given Lewis number are determined by the channel width; section 4 presents symmetric and non-symmetric flames oscillating due to the coupling with acoustic waves; section 5 analyses the frequency of these oscillations and section 6 explains the different oscillating behavior of symmetric and non-symmetric flames. Sections 7 and 8 introduce the effects of variations in parameters such as the channel width and the dependence of the reaction rate on the density. Finally, section 9 summarizes the main conclusions of our study.

2. Numerical model and simulation method

We consider a premixed flame propagating in a two-dimensional channel with width D and length L, filled with a flammable mixture of fuel and air. The channel walls are assumed to be adiabatic and closed at one end (say the left end) and open at the other end. If a fuel-air mixture at initial temperature T_0 is ignited near the open end of the channel, a flame front will grow and propagate, rapidly reaching the walls as well as the open channel end. After this transient, a single flame will remain, propagating towards the fresh mixture, from right to left, as shown in the sketch in Fig. 1. A parabolic velocity profile will be established in the hot combustion product stream, bringing the combustion products to the exit at the right side of the channel. This non-uniform flow will induce a curvature in the flame, whose magnitude depends on the parameters of the problem. The unburned mixture in the region between the moving flame and the closed end of the channel remains stationary (on average, except for the movement of gas particles produced by sound waves). As we shall show below, the resulting curved flame can be symmetric or non-symmetric.

The exact shape and speed of this flame can be determined numerically by solving the governing equations of the problem. Here, we solve the 2D conservation equations for mass, momentum, energy and fuel mass fraction. We will assume a one-step irreversible chemical reaction F+O $\rightarrow$ P where F is the deficient reactant, so that the reaction rate depends on its mass fraction, Y_F. Neglecting body forces, radiation heat losses and heating by viscous dissipation, the two-dimensional governing equations are:

$$\frac{\partial \rho}{\partial t} + \frac{\partial \rho u_i}{\partial x_i} = 0 \tag{1}$$
$$\frac{\partial \rho u_i}{\partial t} + \frac{\partial \rho u_i u_j}{\partial x_j} = -\frac{\partial p}{\partial x_i} + \frac{\partial \tau_{ij}}{\partial x_j} \tag{2}$$
$$\frac{\partial \rho e_t}{\partial t} + \frac{\partial \left(\rho e_t + p\right) u_i}{\partial x_i} = \frac{\partial u_i \tau_{ij}}{\partial x_j} - \frac{\partial q_i}{\partial x_i} + Q\, \dot{\omega}_F \tag{3}$$
$$\frac{\partial \rho Y_F}{\partial t} + \frac{\partial \rho Y_F u_i}{\partial x_i} = \frac{\partial}{\partial x_j}\left(\rho\, \mathcal{D} \frac{\partial Y_F}{\partial x_j}\right) - \dot{\omega}_F \tag{4}$$

Here u_i are the components of the gas velocity, ρ its density, p the pressure, Y_F the fuel mass fraction and e_t the total (non-chemical) energy, defined as $e_t = \frac{1}{2} u_k u_k + p/\rho\,(\gamma - 1)$, with $\gamma = c_p/c_v$, the relation of heat capacities, assumed constant, and where the perfect gases equation of state: $p = \rho \mathcal{R} T = \rho (c_p - c_v) T$ is used.

Equations 1-4 are completed by the definitions of τ_{ij}, the viscous stress tensor $\tau_{ij} = \mu \left(\partial u_i/\partial x_j + \partial u_j/\partial x_i - \frac{2}{3}\delta_{ij} \partial u_k/\partial x_k\right)$, and q_i, the components of the heat flux vector, modelled via a Fourier law as: $q_i = -\lambda \partial T/\partial x_i$, where $\lambda = \mu c_p/Pr$ is the thermal conductivity of the gas mixture, defined as a function of the mixture viscosity μ, its heat capacity c_p and a constant Prandtl number Pr. The viscosity and conductivity are assumed to vary with temperature, as $\mu/\mu_0 = \lambda/\lambda_0 = (T/T_0)^{0.7}$, while the fuel diffusivity $\mathcal{D}$ appearing in Eq. 4 is related to the thermal diffusivity and the thermal conductivity via a constant Lewis number Le as $\mathcal{D} = \mathcal{D}_T/Le = \lambda/\left(\rho c_p Le\right)$ and depends on temperature as $\rho \mathcal{D}/\rho_0 \mathcal{D}_0 = (T/T_0)^{0.7}$. The subscript 0 stands here and throughout the paper for quantities evaluated in the fresh gas mixture.

Finally, the fuel consumption rate per unit volume and time, $\dot{\omega}_F$, is described by an Arrhenius law:

$$\dot{\omega}_F = \mathcal{B}\, \rho^n\, Y_F\, \exp(-E_a/\mathcal{R}T), \tag{5}$$

where E_a is the activation energy and $\mathcal{B}$ is the pre-exponential factor. The exponent n, taking values $n = 1$ and 2 is used here to represent Arrhenius models proportional to either ρ or ρ^2. This dependence has an effect on the flame-acoustics interaction, as will be shown in section 8. Even if $n = 2$ could be more appropiate to represent an order-two global reaction rate proportional to the product of the partial densities of the deficient and the abundant reactant, because most of the works on flame-acoustics interaction use an Arrhenius expression proportional to ρ, we maintain $n = 1$ in this work, unless otherwise specified. We introduce the Zel'dovich number $\beta = E_a\,(T_a - T_0)\,/\,(\mathcal{R}\,T_a^2)$ and the thermal expansion parameter $q = T_a/T_0$, the standard parameters characterizing Arrhenius models, with T_a the adiabatic flame temperature. The heat produced per unit volume and time, $Q\,\dot{\omega}_F$, is given by the factor $Q = (T_a - T_0)c_p/Y_{F0} = (q-1)T_0 c_p/Y_{F0}$, where Y_{F0} represents the fuel mass fraction in the fresh gas mixture.

We solve a dimensionless version of Eqs. 1-4, scaled with the thermal flame thickness of the planar flame, defined as $\delta_T = \mathcal{D}_{T0}/S_L$ (with $\mathcal{D}_{T0}$ the thermal diffusivity of the fresh gas mixture, $\mathcal{D}_{T0} = \lambda_0/\,(\rho_0 c_{p0})$, and S_L the laminar planar flame speed), a time scale δ_T/c_0 (with c_0 the speed of sound in the fresh gases, $c_0 = \sqrt{\gamma p_0/\rho_0}$), and the fresh gases reference state given by ρ_0, T_0, μ_0, Y_{F0} and c_{p0}. For this dimensionless version of the equations the only free parameters are Le, Pr, q, β, γ, a Damköhler number Da related to the pre-exponential factor $\mathcal{B}$ as $Da = \mathcal{B}\rho_0^{n-1}\delta_T/c_0$, and an acoustic Reynolds number $Re_{\mathrm{ac}} = \delta_T\, c_0/\nu_0$, which relates the thermal flame thickness, the sound speed in the fresh gases c_0, and the fresh gases kinematic viscosity $\nu_0 = \mu_0/\rho_0$. In this work we will assume Lewis number $Le = 1$, Prandtl number $Pr = 0.7$, the relation of heat capacities $\gamma = 1.4$, a value of the thermal expansion parameter $q = 8$ and a value of the Zel'dovich number $\beta = 10$. These are representative values for hydrocarbon combustion. The acoustic Reynolds number is chosen to be $Re_{\mathrm{ac}} = 476.19$. The Damköhler number Da determines the burning speed of the planar unstretched flame, S_L. Here it is chosen so that the flame Mach number $Ma = S_L/c_0$ takes the value $Ma = 0.003$ (and thus it takes different values for $n = 1$ and $n = 2$).

The computational domain is a rectangle of width D and length L, as shown in Fig. 1. In this work we vary the channel width in the range $D = 10\,\delta_T - 80\,\delta_T$ (this would correspond to $1 - 8$ mm for typical thermal flame thicknesses of the order of 0.1 mm). The channel length is varied from $L = 800\,\delta_T$ to $5000\,\delta_T$, that would correspond to about $80 - 500$ mm. In all these cases the computational domain is discretized on uniform Cartesian grids containing typically 100×2000 cells for a channel with $D = 40\,\delta_T$ and $L = 800\,\delta_T$. Notice that the parameter δ_T defined above is just a length scale, not a measure of the real flame thickness. A closer measure of the flame thickness is given by $\delta_L = (T_a - T_0) \,/\, \frac{dT}{dx}\big|_{max}$, which is about five times larger according to [32] (for the present planar flame, in particular, we obtained $\delta_L = 5.9\,\delta_T$). In the present calculations we have a grid resolution about 15 times smaller than δ_L. Grid refinement studies have been conducted for selected cases, showing no appreciable differences in the results of simulations when the grid resolution was doubled or even quadrupled (see AppendixA). For some particular cases a grid with finer resolution was required; this will be discussed in the text as these cases are presented. The time step is determined by a CFL condition based on the sound speed with a value 0.5 for the CFL factor.

Adiabatic, no-slip, no-flux boundary conditions are imposed at the channel walls (the effect of heat losses will be considered elsewhere). At the open channel end a pressure node with constant pressure equal to the atmospheric pressure ($p = p_{atm}$) is set, as should correspond to an outlet open to the atmosphere. Note that the constant pressure boundary condition implies reflection of sound waves at the open end [32, 33]. Therefore the flame-sound interaction will be different to that described in [29, 30], where non-reflecting boundary conditions were applied at the channel exit and the flame-acoustics interaction happens mainly due to the acoustic mode between the flame front and the closed end wall. Here, because of the reflection of sound waves at the exit, the acoustic mode between the flame front and the open end also affects the flame-acoustics interaction. This is, in our opinion, a more realistic boundary condition for an open tube, and it has been used in several numerical studies concerning acoustic flame instabilities [34–36]. The NSCBC methodology [33] is used to implement the boundary conditions. It should be mentioned that in the case of very strong acoustic oscillations, the flow direction in the burnt gases may be occassionally inverted, so that the outlet becomes an inlet. When this is the case, the entering gas is considered to have the composition and temperature of burnt gases.

The calculations are initialized using a planar flame solution, located at a distance $x_0 = 8\,\delta_T$ from the open end, as in [29, 30]. This avoids the need to solve for the ignition period, which would imply very small times steps and therefore high computational costs. Three kinds of simulations will be presented below: 1) simulations starting from a planar flame and using the full computational domain, $0 < y < D$; 2) simulations in the full computational domain starting from a planar flame with an added non-symmetric perturbation, in the shape of a circular hot spot centered at $(x_c = x_0 - \delta_T; y_c = 3D/4)$ and with radius $R = \delta_T$, so that the perturbed initial temperature is $T(x, y) = T_{\text{planar}}(x, y) \left[1 + 6 \exp\left(-\left((x - x_c)^2 + (y - y_c)^2\right)/2R^2\right)\right]$, where $T_{\text{planar}}(x, y)$ is the unperturbed initial planar flame temperature; and 3) simulations using half the computational domain, $0 < y < D/2$, and imposing symmetry along the central axis $y = D/2$. This last kind of simulations is used to force a symmetric solution in cases where the symmetric flame might be unstable.

While the constant-pressure boundary condition at the duct exit and the viscosity dependence with temperature are two differences with the simulations presented in [29, 30], the main difference between those papers and the present work is our consideration of both symmetric and non-symmetric solutions for the propagating flames, as explained in the introduction.

To solve the system of equations Eqs. 1-4, together with the mentioned boundary conditions, we use the compressible solver NTMIX3D, a parallel solver designed for the direct numerical simulation of flames and turbulent reacting flows described in [37] and thoroughly validated (see e.g. [37–39]), using a sixth-order accuracy compact finite differencing-scheme [40] and third-order Runge-Kutta time integration.

In analysing the results, in what follows we shall measure the flame consumption speed (normalized with the flame speed of the corresponding planar

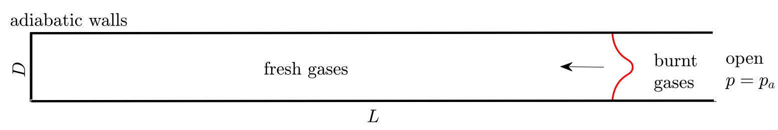

Figure 1: Sketch of the problem.

unstretched flame S_L) by the integral:

$$S_c/S_L = \frac{1}{\rho_0 Y_{F0}\, D\, S_L} \int_0^D \int_0^L \dot{\omega}_F \, dxdy. \tag{6}$$

A symmetry factor defined as:

$$|S| = \frac{1}{(T_a - T_0)\, DL} \int_0^{D/2} \int_0^L |T(x,y) - T(x, D-y)| \; dxdy, \tag{7}$$

so that it is equal to zero for perfectly symmetric flames, shall be used to distinguish symmetric and non-symmetric solutions. It is obvious that $|S|$ is exactly zero (within the numerical accuracy) for symmetric distributions and non-zero for non-symmetric ones.

3. Symmetric and non-symmetric solutions.

When a flame propagates in a channel in a quiescent mixture, the hot products are put in motion and, because of friction with the walls, a parabolic flow is established in the hot gas stream. This flow induces a curvature in the flame, increasing its surface and, consequently, its consumption speed. Heat losses to the wall may contribute also to curving the flame, but for an adiabatic channel the final shape depends only on the channel width, the thermal expansion parameter and the mixture Lewis number. As reported in [19], for a flame with $Le = 1$ freely propagating in a channel with imposed flow rate m and with a given thermal expansion rate q, there is a critical channel width below which the flames are always symmetric and above which two solutions are possible: a symmetric or a non-symmetric flame. It has been shown that the symmetric flame becomes unstable and a non-symmetric flame is generated during the growth of small perturbations [19]. Symmetric and non-symmetric flames have different flame surface and therefore different consumption speeds.

Of course the two kind of solutions may exist as well in the present case where flames with $Le = 1$ propagate in a channel from an open to a closed end. This is illustrated in the temperature distributions presented in Fig. 2, corresponding to the symmetric and non-symmetric solutions for a $Le = 1$, $q = 8$ flame propagating in a channel of width $D/\delta_T = 20$ and $L/\delta_T = 800$.

Figure 3 presents the consumption speed S_c/S_L and the symmetry factor $|S|$ for flames with $Le = 1$ and $q = 8$ propagating from the open to the closed end in several channels with a fixed length $L/\delta_T = 800$ and increasing widths $D/\delta_T = 10 - 30$. The solid lines correspond to simulations in a half channel and therefore to imposed symmetric conditions. The dashed lines correspond to simulations in the full domain starting from a planar flame plus a non-symmetric perturbation as described in section 2. For the narrower channels the flame is planar, thus $|S| = 0$, and the propagating speed is equal to that of the planar unstretched flame, $S_c/S_L = 1$. As the channel is made wider the flames acquire a curvature and the flame speed adopts values $S_c/S_L > 1$. For $D/\delta_T < 17$ all the computed flames have symmetric shapes, as shown by the zero value of the symmetry factor $|S|$. For wider channels, $D/\delta_T >= 17$, symmetric and non-symmetric solutions are mathematically possible (even

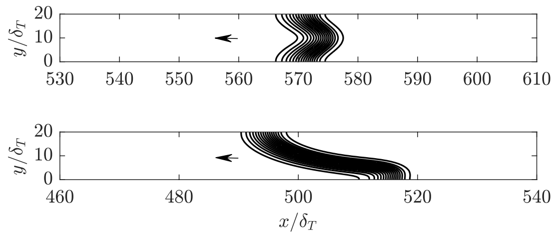

Figure 2: Flame structures obtained in the simulation of a flame with $Le = 1$ and $q = 8$ propagating from the open to the closed end of a channel with $D/\delta_T = 20$ and $L/\delta_T = 800$. The flames are represented by isotherms plotted at steps $\delta T/(T_0(\gamma - 1)) = 1$ and correspond to the same instant in the flame propagation.

if only the non-symmetric flame is stable), and the non-symmetric solution burns faster than the corresponding symmetric flame. Note that all the flames in Fig. 3 propagate steadily after some transient. Even if some oscillations can be observed in the flame speed at the initial propagation stages (see for example the symmetric flame corresponding to $D/\delta_T = 30$), these are rapidly damped, due to dissipative effects.

For $Le = 1$, $q = 8$ and adiabatic walls, the critical channel width for which non-symmetric flames exist lays between $D/\delta_T = 16$ and $D/\delta_T = 17$. Note that in simulations done assuming constant viscosity (independent of temperature), we found that the critical channel width was between $D/\delta_T \approx 5.5$ and $D/\delta_T \approx 6$, which agrees with the values reported in [19] for approximately the same parameter set. The temperature-dependent viscosity of the present study, results in a different effective thickness of the flame and therefore a different value of the critical channel thickness for symmetry breaking. It should be noted that in the present study the definition of the thermal flame thickness, δ_T, is based on the cold gas transport parameters.

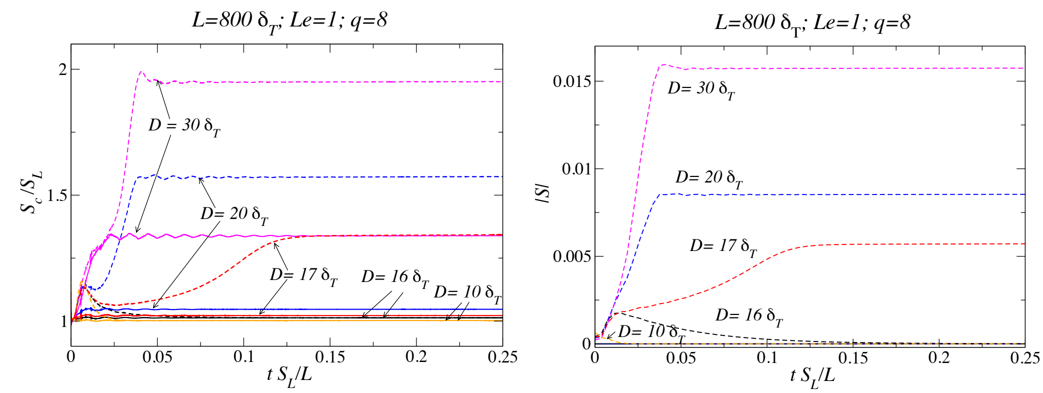

Figure 3: The flame consumption speed, S_c/S_L, and the symmetry factor, $|S|$, for flames with $Le = 1$ and $q = 8$ propagating in channels with length $L/\delta_T = 800$ and different widths.

4. Oscillating flames

As the channel is made wider, self-sustained oscillations appear as a result of flame-sound interaction. No oscillation occurs if a zero Mach number formulation is used (this was verified in a separate set of simulations). Figure 4 presents the time evolution of the normalized consumption speed, S_c/S_L, the mean flame position, x_f, scaled with L, and the pressure at the channel closed end, p_w/p_a, for a flame propagating in a channel with $D/\delta_T = 40$ and $L/\delta_T = 800$. Note that $L/\delta_T = 800$ is the smallest length for which oscillations are detected for this channel width, for shorter channels initial oscillations are rapidly amortiguated by dissipative effects, as was the case with the thinner channels of Fig. 3. The flame consumption speed is computed using Eq. 6, and the pressure at the closed end is measured at the centre of the end wall. We estimate the mean flame position via the burnt volume fraction, V_b (defined as the fraction of volume in the channel -or area in these 2D

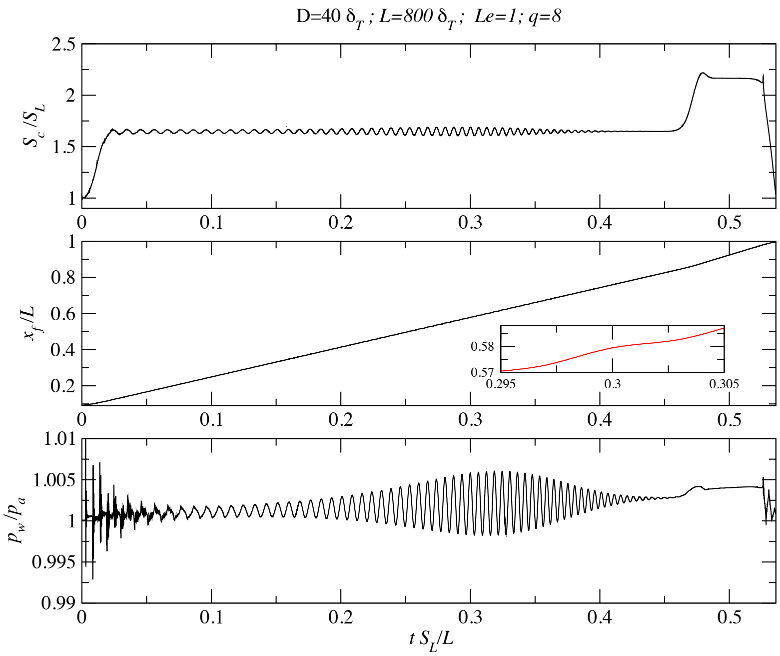

Figure 4: The flame consumption speed, S_c/S_L, flame position, x_f/L, and pressure at the channel closed end (left wall), p_w/p_a, for a flame propagating in a channel of width $D/\delta_T = 40$ and length $L/\delta_T = 800$. The inset corresponds to a zoom of the x_f/L curve, where weak oscillations of the flame position may be appreciated.

calculations- where the temperature is above the value $T_* = 1/2(T_a - T_0)$), as: $x_f/L = V_b/(DL)$. The mean flame position increases from $x_f/L = 0.1$, corresponding to the initial condition, to $x_f/L = 1$ as the flame reaches the end wall. This is an average measurement of the flame advancement, different to what would be measured by tracking the position of a specific flame point. Indeed a flame point may oscillate about a fixed position without changing the burnt volume fraction.

Starting from the initially planar flame, for which the consumption speed is $S_c = S_L$, the flame acquires a curved tulip shape as it propagates along

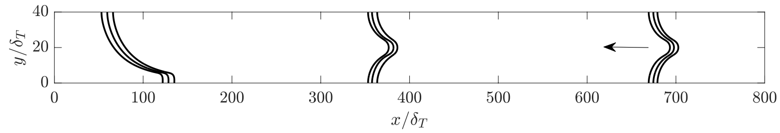

Figure 5: Isotherms corresponding to $T_* = 1/2\,(T_a - T_0)$ for a flame propagating in a channel of width $D/\delta_T = 40$ and length $L/\delta_T = 800$. The three flame groups correspond to the beginning (symmetric flame with small oscillations), the middle (symmetric flame, with maximum oscillations) and the end of the simulation (non-symmetric, steadily propagating flame). In the three cases the plotted isosurfaces are separated by the same time delay, corresponding to half the period of the maximum amplitude cycle).

the channel and accelerates, reaching a speed of about $S_c = 1.65\,S_L$. Then it starts oscillating, and this oscillation amplifies, becoming maximal when the flame is at the second half of the channel. Changes in the flame shape are small, but still appreciable in Fig. 5, where isolines of constant temperature ($T_* = 1/2(T_a - T_0)$), representing the flame surface, are plotted for three different stages of the flame propagation: near the beginning, at the cycle of maximal amplitude and near the end of the channel. In the three groups the plotted isosurfaces are separated by the same time delay, corresponding to half the period of the maximum amplitude cycle. The maximum amplitude cycle occurs at a location after the middle of the channel, at about $x_f/L = 0.55$. After that, the amplitude of the oscillations decays. We plot in Fig. 6 the flame consumption speed oscillations about the mean value corresponding to the curved flame, $S'_c = (S_c - 1.65S_L)/S_L$, and the pressure oscillations about the atmospheric pressure value, $p'_w = (p_w - p_a)/p_a$. Note that the value of S'_c at initial times is $S'_c = (S_L - 1.65S_L)/S_L = -0.65$ and lays out of the y-axis range of the figure. We can see in this figure that the pressure

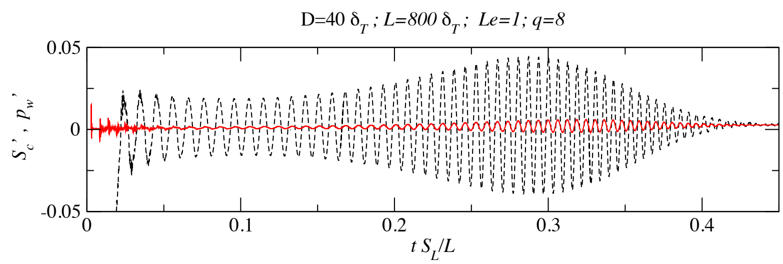

Figure 6: In-phase oscillations in the flame consumption speed S_c' (dashed lines) and the pressure at the end wall p_w' (solid lines) for a flame propagating in a channel of width $D/\delta_T = 40$ and length $L/\delta_T = 800$.

measured at the end wall oscillates in phase with the flame speed, which, according to Rayleigh's criterion, is a necessary condition for self-sustained thermo-acoustic instabilities.

Before reaching the end wall, a large change in flame consumption speed occurs. This corresponds to the flame transitioning to a non-symmetric slanted shape, as can be seen in Fig. 5. For this slanted flame, the flame surface and therefore the consumption speed are larger. This flame propagates steadily, showing no oscillations, at a speed about $2.2S_L$, and rapidly reaches the end wall and extinguishes as the fuel is completely consumed. At the final propagation stages near the end wall, a small decceleration, followed by a sudden acceleration precede the final extinction. This corresponds to a reduction in flame surface after the flame tip reaches the wall, followed by the fast engulfment and consumption of a blob of remaining fuel at the channel corner. These changes in flame speed, which can be appreciated in Fig. 4 top, produce noise, as can be seen in Fig. 4 bottom.

Figure 7 presents pressure and gas velocity profiles at the central horizontal channel axis. The profiles in Fig. 7 a) correspond to four different instants along the flame propagation: $t\,S_L/L = 0, 0.15, 0.30$ and 0.45. As the flame propagates in the channel, a negative pressure gradient is established between the flame position and the open channel end, which opposes the wall friction and pushes the hot gases towards the channel exit, with maximum speeds at the central axis of the order of $U \approx 18 S_L$. The pressure profile between the flame and the closed-end wall is uniform for $t\,S_L/L = 0.15$ and 0.45, with a pressure level that grows as the flame travels towards the wall. This uniform pressure corresponds to a negligeable gas velocity before the flame, indicating that the fresh gases are at rest and uniformly compressed as the flame advances. The pressure between the flame and the end wall at $t\,S_L/L = 0.30$ (dashed-dotted line) is not constant, it presents a non-uniform gradient which corresponds to a pressure wave, as we can see by inspecting Fig. 7 b).

The pressure and velocity profiles in Fig. 7 b) correspond to half the cycle of maximum amplitude shown in Fig. 5. The solid line corresponds to the instant in this cycle when the flame surface is minimum, that is, the instant of maximum negative amplitude in the flame speed oscillations. The dashed-dotted line corresponds to the instant when the flame surface is maximum, that is, the maximum amplitude in the flame speed oscillations. Finally, the dashed line profiles correspond to an intermediate time between these two, where the flame surface (or speed) takes the mean value between oscillations. We can see that, because of these pressure wave oscillations, the pressure at the flame position and the pressure gradient between the flame and the channel open-end oscillate. These oscillations are small, so that the pressure gradient does not change sign and the flux between the flame and the open end remains positive (towards the channel exit). Because this particular channel is rather short, the pressure difference needed to push the hot gases through the open end is small. However, the pressure gradient between the flame and the closed-end wall oscillates with a larger amplitude and changes its sign, driven by pressure waves travelling between the flame and the closed wall. This oscillating pressure gradient induces a small flux in the fresh gases, switching between positive and negative values opposed in phase to the pressure oscillations. In summary, the fresh gases between the flame and the channel end wall are at rest except for small oscillating fluxes induced by pressure waves.

We have seen that, as described in [26, 27], oscillations in the flame surface (and speed) are driven by acoustically-induced accelerations of the flow just upstream the flame, linked to acoustic waves propagating between the channel end wall and the flame. Waves are reflected at the closed channel end and (partially) at the flame surface as well as at the open channel end. If these waves are amplified by the flame, and in its turn the flame response is strong enough and in phase with the sound waves, then oscillations may grow, leading to self-sustained instabilities. However, if the flame response is weak then oscillations can be dissipated.

It seems clear from these results and those of the precedent section that a minimum channel width is needed for the flame to oscillate. For a channel with $D/\delta_T = 30$ oscillations are small and rapidly dissipated (see Fig. 3) . For a channel with $D/\delta_T = 40$ persistent oscillations are detected. This is a consequence of the increase in the flame curvature: the response of a

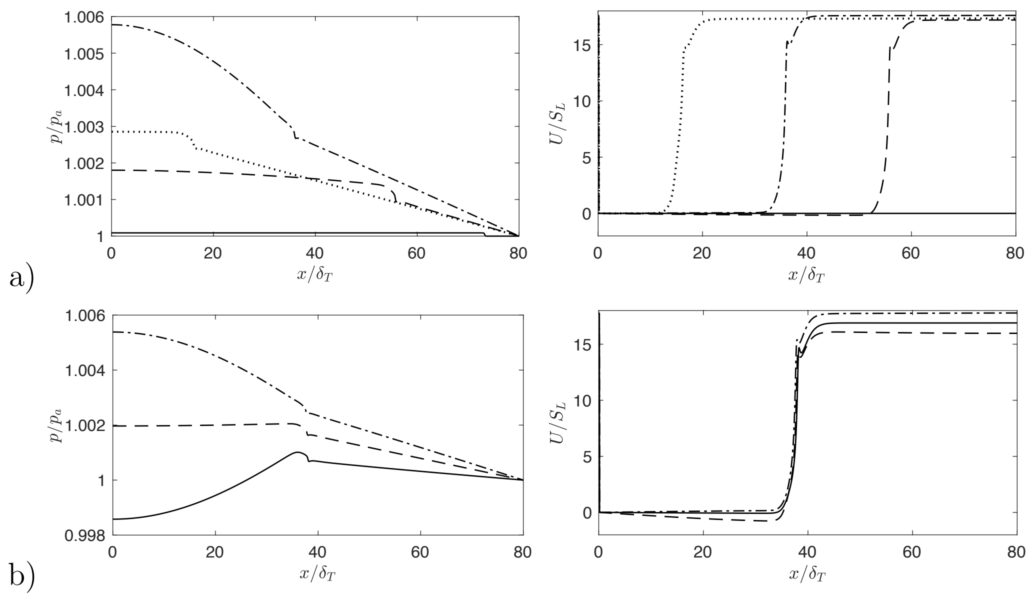

Figure 7: Pressure and gas velocity at the horizontal central axis for a flame propagating in a channel with $D/\delta_T = 40$ and $L/\delta_T = 800$. a): Four instants along the flame propagation (solid, dashed, dashed-dotted and dotted lines, corresponding, respectively, to $t\,S_L/L = 0, 0.15, 0.30, 0.45$) b) Three instants in the cycle of maximum amplitude of the oscillating flame of Fig. 5. The three profiles correspond to the instant of smallest flame surface (solid), to the instant of largest flame surface (dashed-dotted) and to an intermediate time. They represent thus half a cycle.

planar flame to acoustic wave oscillations is very weak [41, 42], as the flame becomes curved, the flame response to oscillations becomes stronger, and for a certain value of the curvature the flame response is strong enough to amplify initial perturbations and compensate the dissipation of acoustic energy by viscous effects. Moreover, we have also observed that a minimum channel length is needed for the oscillations to persist: for the present channel width, oscillations only appear for a minimum length of $L/\delta_T = 800$. As we shall see later, this is related to the acoustic modes of the channel, which determine the possible frequencies of acoustic waves in the channel for a given channel length. Only when pressure oscillations at these frequencies are able to produce an amplified flame response we will find a coupling between the flame and the acoustics.

The question now arises of why when the flame becomes non-symmetric oscillations cease as seen in Fig. 4. Two possible answers can be anticipated: 1) it could be because its shape preclude oscillations (if the non-symmetric flame response is too weak for a flame-sound resonance to appear) or 2) it may be because it appears at a late stage, where the flame is at a short distance from the wall and the corresponding frequency of acoustic oscillations is too fast to create the adequate flame response. A partial answer can be given by doing a second simulation in which a non-symmetric perturbation is added to the initial planar flame condition, to trigger an earlier transition towards the non-symmetric solution. The results of this simulation are plotted with dashed lines in Fig. 8. Solid lines correspond to the results already presented in Fig. 4, in which no perturbations were added to the initial condition and the transition to the non-symmetric solution is triggered by perturbations induced by the numerical method. The top plot in Fig. 8 presents the consumption speed for the two simulations, while the bottom plot presents the unsigned symmetry factor. It is clear that the non-perturbed solution (solid black lines) is symmetric until very near the end of the simulation and that the change in consumption speed is linked to the flame becoming non-symmetric. In the perturbed case (dashed red lines) the flame switches to the non-symmetric solution much earlier, at a reduced time about 0.6; it is non-symmetric from the early stage and it propagates steadily, with no oscillations, along the channel. There is no position in the channel where the non-symmetric flame response is amplified by the acoustics of the channel and acoustic instabilities never appear (in this channel) for the non-symmetric solution.

As the channel length is increased, the amplitude of oscillations of the symmetric flames becomes higher, and the flame position where oscillations occur moves towards the end of the channel, as can be seen in Fig. 9 a) for $L/\delta_T = 1200$. For a length $L/\delta_T = 1600$ the non-symmetric flame also oscillates, even if with a small amplitude. Notice that the initial steadily propagating symmetric flames are identical in curvature and consumption speed in the shorter and the longer channels (the same occurs with the non-symmetric flames). However, the flames oscillate in one channel and not in the other one. As we shall see later, this is related to the acoustic eigen modes of the channel, which depend on the channel length.

Figure 9 c) presents a visualization of the maximum amplitude cycle for the symmetric flames in the three channels. The three plots in this figure present surfaces of constant temperature ($T_* = 1/2(T_a - T_0)$) for the cycle that

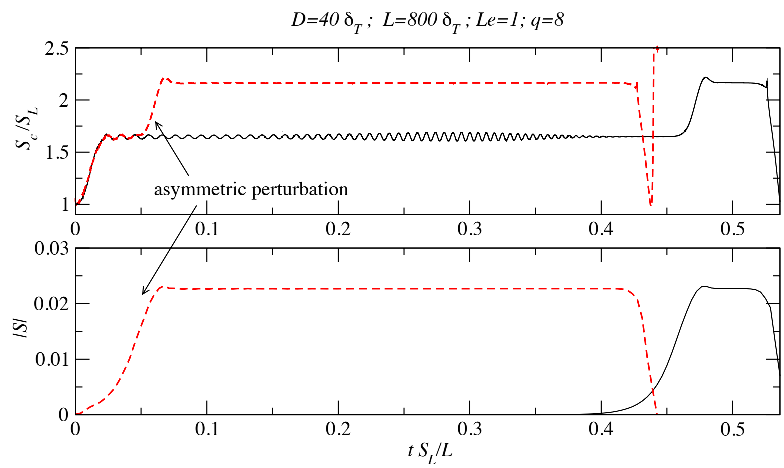

Figure 8: The flame consumption speed S_c/S_L and symmetry factor $|S|$ in the simulations of a flame propagating in a channel of width $D/\delta_T = 40$ and length $L/\delta_T = 800$. The solid black lines correspond to the simulation in Fig. 4, with perfectly symmetric initial conditions corresponding to a planar flame, the dashed red lines correspond to non-symmetrically perturbed initial conditions, triggering a faster transition to the non-symmetric solution.

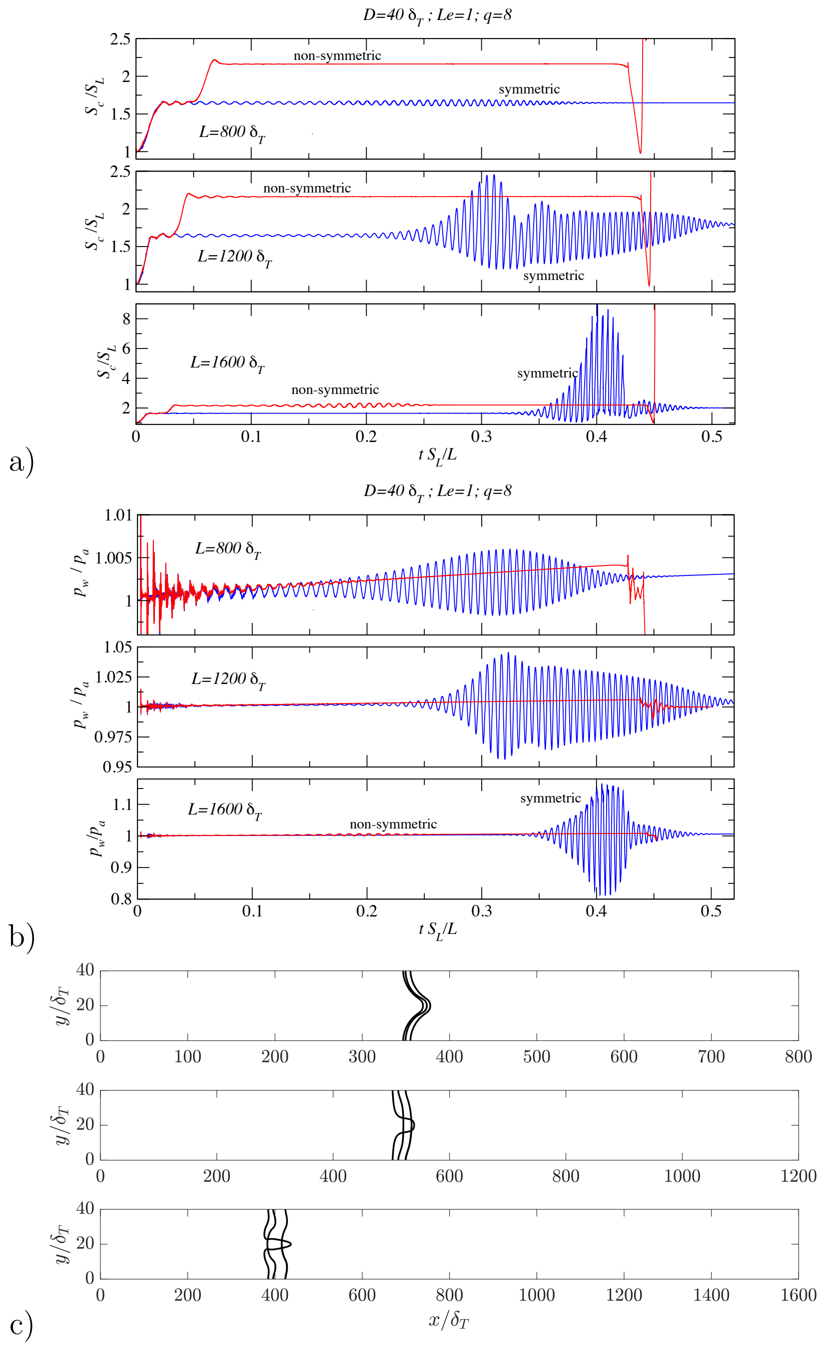

Figure 9: a) Flame consumption speed, b) pressure at the end wall and c) isotherms at $T_* = 1/2\,(T_a - T_0)$ at the maximum amplitude cycle for a flame propagating in a channel with $D/\delta_T = 40$ and length $L/\delta_T = 800, 1200$ and 1600. Blue lines correspond to simulations with imposed symmetry, red lines to simulations in the full domain with non-symmetric initial perturbations.

corresponds to the maximum amplitude of oscillations in the flame speed. For the symmetric flame in the $L/\delta_T = 800$ channel (top), this corresponds to a location just after the mid-channel, and the oscillations are small, resulting in very small changes in the flame shape, as already presented in Fig. 5. For the symmetric flame in the channel with $L/\delta_T = 1200$ (middle) the oscillation of maximum amplitude occurs again just after the mid channel and presents important changes in the flame shape, which is neary planar at the minima of the cycles. Finally, for the symmetric flame in the $L/\delta_T = 1600$ channel (bottom), the peak oscillations occur near the end of the channel, and correspond to very large changes in the flame shape and surface.

Interestingly, as we plot the pressure at the closed channel end for these solutions (Fig. 9 b)), we find that while for the shorter channel the amplitude of pressure oscillations is of the order of 5×10^{-3} the atmospheric pressure (or about 500 Pa), it increases with the channel length and becomes more than an order of magnitude larger, about one tenth of the atmospheric pressure (or 10000 Pa) for the longer channel. These are the orders of magnitude reported in the experiments in [21] and [24, 25] for primary and secondary instabilities, respectively. As commented in the introduction, in those experiments the transition is related to changes in the burning mixture equivalence ratio. In the present configuration, the transition from small to large amplitude oscillations is rather related to an increase in the channel length for a fixed mixture composition.

We have seen in Fig. 9 that as the channel is elongated, the non-symmetric flames start oscillating, initially with very small amplitudes, barely visible for the channel with $L/\delta_T = 1600$. For even longer channels the non-symmetric flame oscillations increase in amplitude, as can be seen in Fig.10. For the case $L/\delta_T = 2400$, both the symmetric and the non-symmetric solutions oscillate, the symmetric flame with a slighty larger amplitude. The non-symmetric flame oscillations occur in the first half of the channel while the symmetric flames oscillate near the channel end. This can be appreciated in Fig. 10 c), where the isotherms at the maximum amplitude cycle for the non-symmetric and the symmetric flames in each channel are represented. For the channel with $L/\delta_T = 4000$, the non-symmetric flame oscillations increase in amplitude and the symmetric flame almost ceases oscillations. As the channel is further lengthened, to $L/\delta_T = 5000$, the symmetric flame starts oscillating again, with an amplitude similar to that of the non-symmetric flame. An explanation for this behavior shall be given in the next two sections, as we analyze the period of the flame oscillations, the acoustic eigen modes of the channel and the flame transfer function.

Pressure oscillations in the channels with $L/\delta_T = 2400$, 4000 and 5000 are of the order of $5 \times 10^{-2} p_a$, about 5000 Pa (see Fig. 10 b)), which corresponds to the amplitudes of secondary instabilities in the experiments of [21, 24, 25].

5. Period of the oscillations and acoustic eigen modes of the channel

We measured the period of the pressure oscillations as the flame propagates along the channels for the cases shown in Figs. 9 and 10, and plot it as a function of the flame distance to the end wall, x/L, in Fig. 11. The period of oscillations is scaled in this figure with the channel length L and the speed of sound in the fresh gases c_0. It decreases with the decrease of the distance

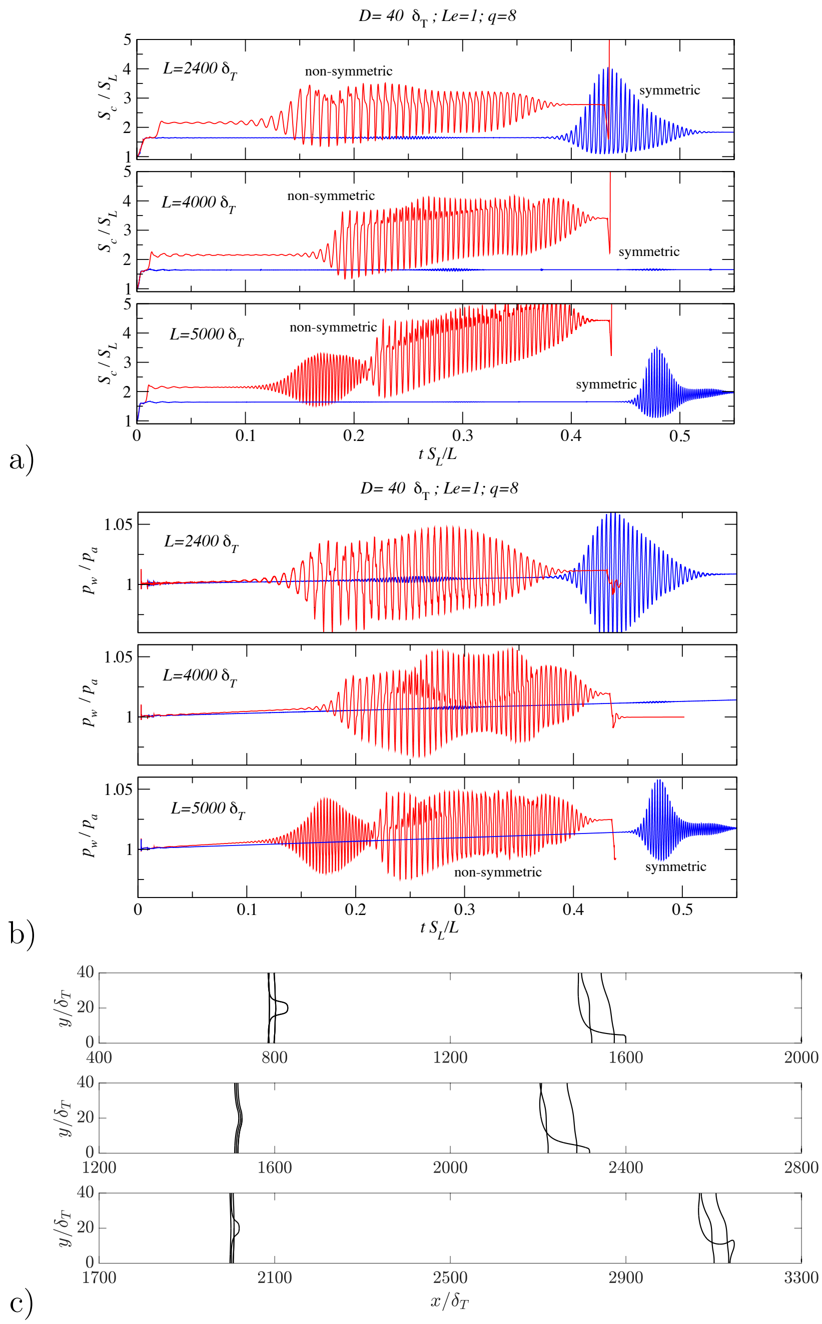

Figure 10: a) Flame consumption speed, b) pressure at the end wall and c) isotherms at $T_* = 1/2\,(T_a - T_0)$ at the maximum amplitude cycle for non-symmetric and symmetric flames propagating in a channel with $D/\delta_T = 40$ and length $L/\delta_T = 2400, 4000$ and 5000. Blue lines correspond to simulations with imposed symmetry, red lines to simulations in the full domain with non-symmetric initial perturbations.

to the wall, this indicates that the oscillations depend on the travelling time of the acoustic signal to the end wall. But instead of a linear decrease, as would be the case if only the distance to the wall was involved, we observe a different dependence with x.

We plot also in this figure the period of the longitudinal acoustic eigen modes in a narrow channel of length L open at one end and closed at the other end and filled partly with a quiescent gas at the conditions of the fresh gases (ρ_0, c_0) and partly with a quiescent gas at the conditions of the burned gases (ρ_b, c_b). The effect of unsteady heat release on the channel acoustics is neglected, and instead of a flame we just assume a surface separating the fresh and the hot gases and located at x (see the sketch in Fig. 12). The eigen mode equation can be obtained easily from the wave propagation equation with boundary conditions corresponding to a closed end at $x = 0$ and an open end at $x = L$ and reads [32, 36, 43]:

$$\tan\left(\frac{\omega x}{c_0}\right)\tan\left(\frac{\omega(L-x)}{c_b}\right) = \frac{\rho_0 c_0}{\rho_b c_b} \tag{8}$$

or

$$\tan\left(\frac{2\pi x}{\mathcal{T} c_0}\right)\tan\left(\frac{2\pi(L-x)}{\mathcal{T} c_b}\right) = \frac{\rho_0 c_0}{\rho_b c_b} \tag{9}$$

for the frequency ω or period $\mathcal{T}$ of the eigen modes. The solutions of Eq. 9 are plotted with red solid lines in Fig. 11 as functions of x for each of the different channels of length L. It is clear that the period of the pressure oscillations in the present results follows closely the prediction of Eq. 9, with only small deviations for the longest channels. This means that, for the present flames and channel geometry, the period of the pressure (and the flame speed) oscillations is fully determined by the acoustics of the channel.

The heat release oscillations do not change the frequency of oscillations. The flame acts as a passive thin planar surface separating gases with different thermoacoustic properties, and even when oscillations are large, as in the longest channels of the present study, deviations from this behavior are only small.

Note that the 'classical' quarter-wave mode between the flame position x and the closed-end wall, which would correspond to a non-reflecting boundary condition at the open end, would give:

$$\omega x/c_0 = \pi/2 \text{ , or } \mathcal{T} c_0 = 4x \tag{10}$$

This expression is also represented in Fig. 11, with a dashed blue line, and only concides with the predictions of Eq. 8 or Eq. 9 for a flame located at the open end of the channel ($x = L$).

6. Flame response to acoustic waves for symmetric and non-symmetric flames

Similarly to what was done in [41, 42], where the response of planar flames to acoustic waves was investigated, we use numerical experiments to investigate the response of symmetric and non-symmetric curved flames to imposed acoustic waves.

For this study, we will solve Eqs.1-4 with the same numerical scheme and grid resolution presented in section 2, but in a reference frame moving with the flame, as explained below. In a first set of simulations we establish two steady flame solutions in a channel of width $D/\delta_T = 40$ and $L/\delta_T = 400$ open at both ends: a non-symmetric flame in the full computational domain and a

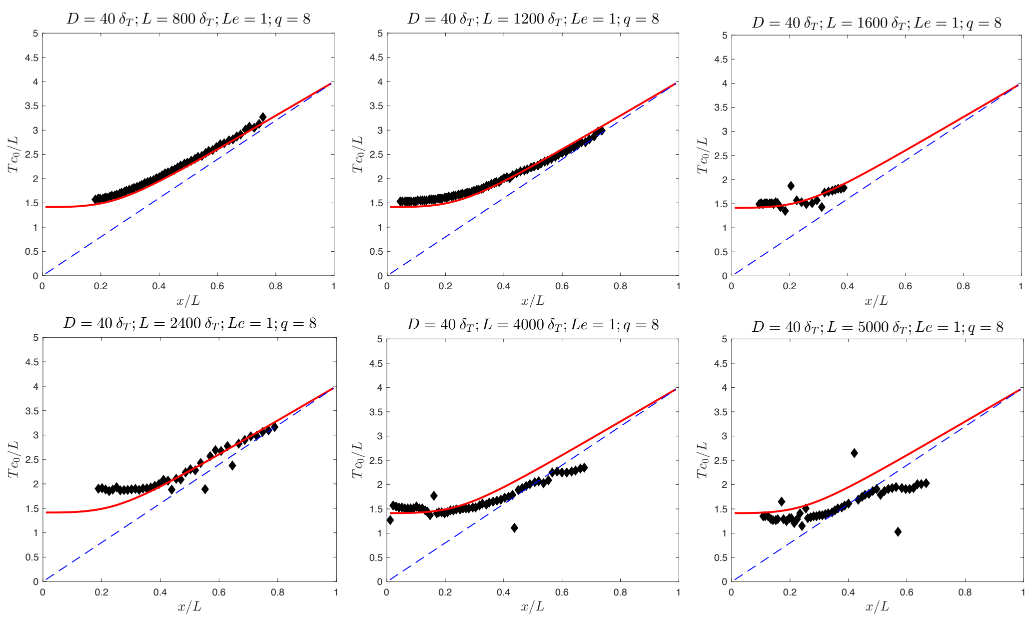

Figure 11: Measured period of the pressure oscillations $\mathcal{T}c_0/L$ as the flames propagate from the open end ($x/L = 1$) to the closed end ($x/L = 0$) for several channels with different L (symbols), compared to the expressions in Eqs. 9 (solid red lines) and 10 (dashed blue lines). For $L/\delta_T = 800, 1200, 1600$ the plots correspond to oscillations of symmetric flames, for $L/\delta_T = 2400, 4000, 5000$ to non-symmetric flames.

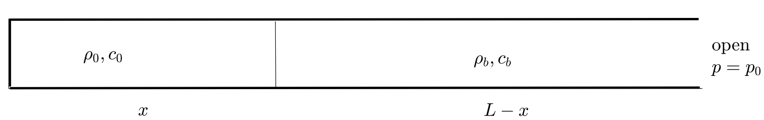

Figure 12: Sketch of an open-closed channel filled with fresh and burnt gases corresponding to the acoustic eigen mode equations Eqs.8 and 9.

symmetric flame in half the computational domain by imposing symmetry at the axis. In the two cases we impose non-reflecting inlet and outlet conditions using NSCBC [33]. The calculations are initiated with a planar flame situated at the middle of the channel. To converge to steady flame solutions, we adopt a reference frame moving with the flame by modifying iteratively the inlet flow rate, so that the final curved flame is stationary in the computational domain, as in [16, 18]. Once the curved flames are established, we force the inlet, superimposing acoustic waves to the inlet flow. These waves have a small amplitude $A_0 = 5 \times 10^{-3} S_L$ and reduced frequencies $f^* = f \delta_T / S_L$ in the range 0.01 to 1. Then we measure the frequency-dependent flame response to these perturbations, that is, the flame transfer function gain, as the relative amplitude of the oscillations in the flame consumption speed A/A_0.

The most delicate point in these simulations is the imposition of boundary conditions at the inlet of the domain. We need to impose an acoustic wave entering the domain and at the same time to make the inlet boundary non-reflecting for possible waves travelling from the interior of the domain towards the inlet. This problem was studied in [44], where it was shown that such a condition can not be fulfilled if velocities are imposed at the inlet. Instead, they proposed a method, called the inlet wave modulation method (IWM), based on NSCBC [33], in which the amplitude of characteristic waves traveling towards the interior of the domain is imposed. Non reflecting conditions are also imposed at the outlet.

Results of these simulations are shown in Fig. 13. For both symmetric and non-symmetric flames the flame response is small ($A/A_0 << 1$) for the highest frequencies and begins to be appreciable for reduced frequencies below ≈ 0.17 in the case of symmetric flames and below ≈ 0.075 for the non-symmetric case. For symmetric flames the response grows slowly as the frequency is decreased. For non-symmetric flames, the response grows more rapidly and reaches a peak near $f^* = 0.05$, before decreasing again for the lowest frequencies.

We include in Fig. 13 the range of reduced frequencies of the longitudinal eigen modes corresponding to several channels, with lengths ranging from $L/\delta_T = 800$ to $L/\delta_T = 10000$, computed using Eq.8. For every channel the smallest frequency corresponds to a position of the flame at the open end of the channel ($x = L$), and the highest frequency to a position at the closed end wall ($x = 0$). For the smallest channel, $L/\delta_T = 800$, Fig. 13 shows that only the symmetric flames have a small but appreciable amplifying response (with $A/A_0 > 1$), and this only for the smallest frequencies; this means that for this channel we should expect small oscillations of the symmetric flames and no oscillations of the non-symmetric flames. This means also that no self-sustained oscillations should be expected (for the present flame parameters) for channels shorter than $L/\delta_T = 800$. As the channels are made longer, e.g. $L/\delta_T = 1200, 1600$, the amplifying response of symmetric flames becomes larger and for the frequencies corresponding to $L/\delta_T = 1600$ non-symmetric flames begin to present an appreciable amplification. Symmetric and non-symmetric flames are both amplified in the channels with $L/\delta_T = 1600$ and $L/\delta_T = 2400$, the amplitude of the response of the non-symmetric flames becomes then dominant for $L/\delta_T = 4000$ and a small amplification is again found also for symmetric flames in the case $L/\delta_T = 5000$.

In summary, Fig. 13 explains the different oscillating behavior of symmetric and non-symmetric flames detected in our simulations in channels of different lengths and depicted in Figs. 9 and 10. A minimum channel length is needed for the flame acoustic instability to be established; for the smallest channels in the present work, which correspond to the highest eigen frequencies, only symmetric flames have a large enough response to lead to self-sustained oscillations. Then, as the channel is made longer, both the symmetric and the non-symmetric flames have a large amplitude response, with different amplification and at different frequencies. According to these results, for even longer channels, longer than those of the present study, for example $L/\delta_T = 10000$, thermo-acoustic instabilities will occur at very small frequencies and both symmetric and non-symmetric flames will oscillate, but with moderate amplitudes. The maximum amplitude of oscillations for the present parameters ($D/\delta_T = 40$, $q = 8$, $Le = 1$) corresponds to a reduced frequency near $f^* = 0.05$, that is, to channel lengths between $L/\delta_T = 1600 - 4000$.

7. Effect of the channel width

Figure 14 presents results for the oscillations of the consumption speed of a flame in a wider channel ($D/\delta_T = 80$) for two different channel lengths. Symmetric and non-symmetric solutions exist again in this case, and present different acoustically-driven oscillations. In the cases shown in Fig. 14, the non-symmetric solutions present very small amplitude oscillations, while the symmetric ones oscillate with large amplitudes. The symmetric flame oscillations are very large in the case with $L/\delta_T = 3200$, and the flame acquires in this case a large surface, as can be seen in Fig. 15 (bottom). The flame in

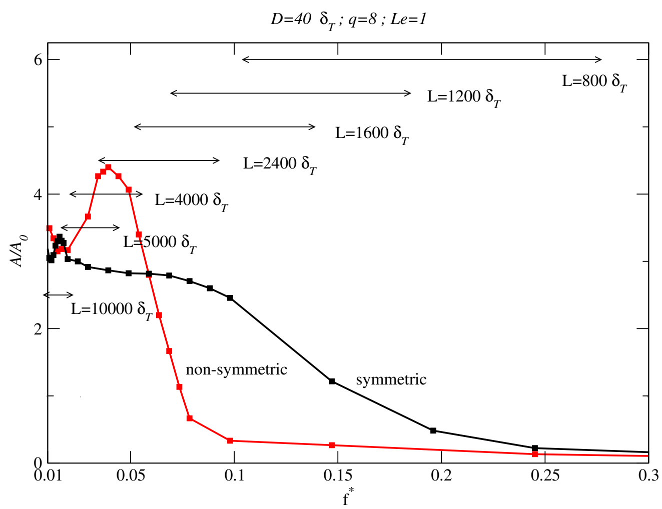

Figure 13: The amplitude of the flame response to imposed oscillations at the inlet (or flame transfer function gain) for symmetric and non-symmetric flames in a channel of width $D/\delta_T = 40$ as a function of the reduced forcing frequency ($f^* = f\delta_T/S_L$). The lines at the top of the figure mark the range of frequencies of the longitudinal acoustic eigen modes of channels of lengths $L/\delta_T = 800 - 10000$.

this figure corresponds to the largest amplitude oscillation in Fig. 14, which is about 30 times the laminar flame speed. Note that for this channel with $D/\delta_T = 80$ and $L/\delta_T = 3200$, the grid resolution had to be increased in order to properly solve the highly corrugated oscillating flame. A grid resolution test, carried out by progressively increasing the number of grid points showed that a mesh with 600×24000 points and a mesh with 800×32000 points gave indistinguishable results. The 600×24000 points mesh (with three times the resolution used in the rest of this work) was therefore kept as adequate for this simulation.

Notice that this very corrugated and very fast flame with violent acoustic oscillations looks similar to that reported in [29] and [30]. It should be mentioned, however, that it corresponds to the symmetric solution, which is not the physical one, as it is unstable. It was forced here by the imposed boundary conditions at the channel axis, but otherwise the solution would have shifted to the stable solution, the non-symmetric flame, which does not present such large oscillations for these narrow channels.

8. Effect of the density exponent in the Arrhenius model

Figure 16 shows the oscillations of the flame consumption speed obtained in channels with $D/\delta_T = 40$ and varying length when the exponent $n = 2$ is used in the Arrhenius model (Eq.5). These results are compared to those obtained using an Arrhenius reaction with $n = 1$, showing that the flame-acoustics interaction changes when this dependence on the density is changed. (Note that when the exponent is changed from $n = 1$ to $n = 2$ the pre-exponential factor in the Arrhenius model is also changed, so that

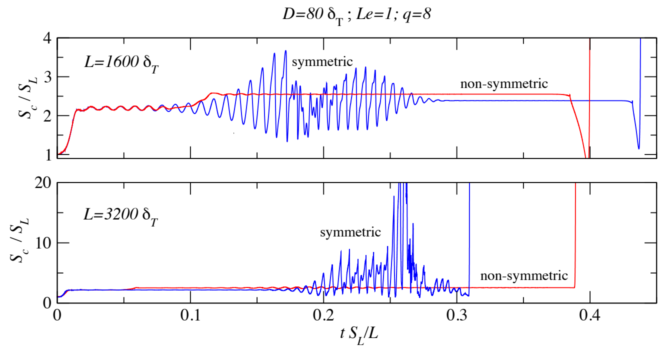

Figure 14: Flame consumption speed in the simulations of a flame propagating in a channel with $D/\delta_T = 80$ and length $L/\delta_T = 1600$ and 3200. Blue lines correspond to simulations in a half-channel with imposed symmetry, red lines correspond to simulations in the full domain with a non-symmetric initial perturbation.

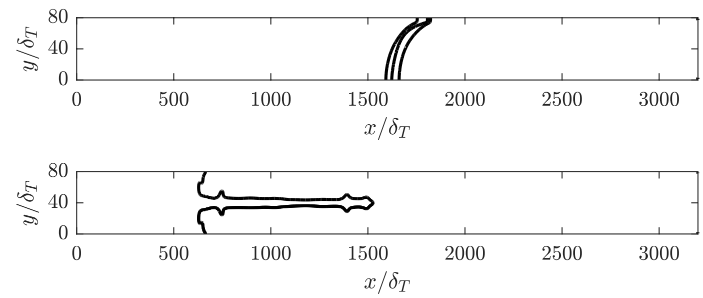

Figure 15: Isocontours of constant temperature $T_* = 1/2\,(T_a - T_0)$ for a flame propagating in a channel with $D/\delta_T = 80$ and length $L/\delta_T = 3200$. The top figure corresponds to the non-symmetric solution maximum oscillation cycle. The bottom figure corresponds to the maximum length flame in the computation in a half channel with imposed symmetry.

the planar flame speed remains unchanged ($S_L = 0.003\,c_0$).) As a general trend, the amplitude of oscillations for both non-symmetric and symmetric flames increases with the value of n, as expected. For the present values of the parameters, it appears that the increase in the amplitude response of symmetric flames is more important. However, the qualitative behavior of the flame-acoustics interaction does not change.

For the case with imposed symmetry with $n = 2$, $D/\delta_T = 40$ and length $L/\delta_T = 5000$, the grid resolution had to be increased. A grid resolution test showed that increasing the grid resolution by a factor 1.6 was enough to obtain reliable results (indistinguishable from those obtained by increasing it by a factor 2). As in the case of symmetric flames with $n = 1$, $D/\delta_T = 80$ and length $L/\delta_T = 3200$ presented in section 7, this need for higher resolution is linked to violent oscillations, reaching flame propagation speeds of up to $30\,S_L$ and corresponding to a highly corrugated flame surface. (Note that for an easier comparison of results, the axis in the bottom right plot of Fig. 16, corresponding to this case, is truncated at a value $S_c/S_L = 12$, even if this flame (blue line) reaches $S_c/S_L \approx 30$.)

9. Conclusions

Numerical simulations of the interaction of flame and acoustics in a narrow adiabatic two-dimensional channel as a $Le = 1$ flame propagates from the open to the close end have been presented. They show that two types of solutions can be found in these unsteady computations, corresponding to a symmetric and a non-symmetric shape, and that the two solutions result in different flame dynamics. The coupling between the flame dynamics and the

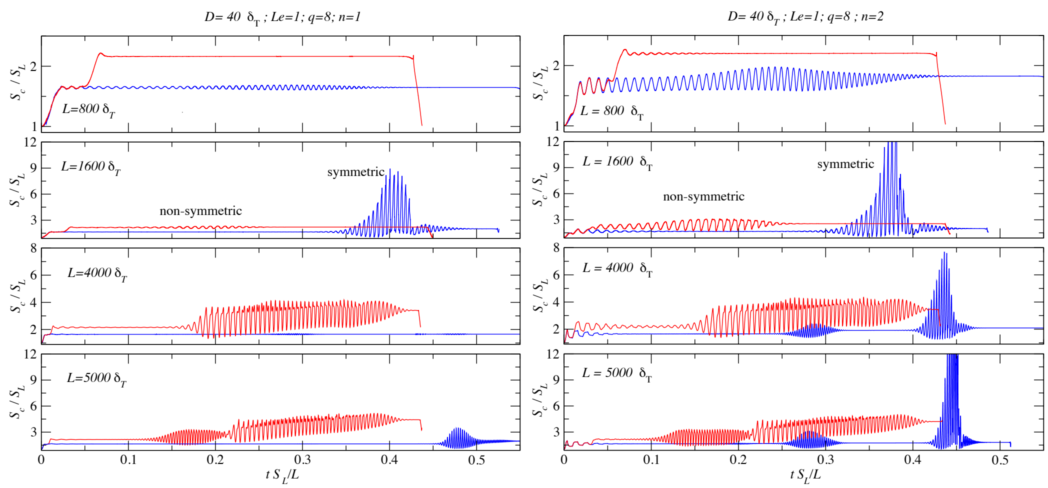

Figure 16: Flame consumption speed in the simulations of a flame propagating in a channel with $D/\delta_T = 40$ and length $L/\delta_T = 800$, 1600, 4000 and 5000. Blue lines: simulations with imposed symmetry, red lines: simulations in the full domain with a non-symmetric initial perturbation. Results in the left column correspond to an Arrhenius model with $n = 1$ and results in the right column to $n = 2$.

acoustic waves in the channel depends on the frequency-dependent response of these curved flames to pressure oscillations, that is, the flame transfer function. The acoustic wave frequencies are determined by the acoustic eigen modes of the channel, which for these narrow channels are longitudinal modes and depend only on the channel length and the fresh/burned gases properties. Symmetric and non-symmetric flames present different flame transfer functions when forced at the frequencies of these acoustic modes. In the present configuration, for $Le = 1$, $q = 8$ and a channel width $D/\delta_T = 40$, the maximum amplification for symmetric flames is found at reduced frequencies of the order of $f^* = f\delta_T/S_L = 0.02$, while non-symmetric flames present the maximum gain at frequencies of the order of $f^* = 0.05$. Moreover, the amplification of non-symmetric flames decreases rapidly with the frequency. so that for the highest frequencies (or the shortest channels) only symmetric flames present oscillations.

In summary, we have shown that the flame-acoustics interaction and the onset of flame acoustic instabilities are different for the symmetric and the non-symmetric solutions. Given that when the two kinds of flames are mathematically possible, and the symmetric solution is usually unstable [19], our results should be a warning against assuming a priori the symmetry of the flame and setting calculations in a computational domain consisting of only a half-channel. In this respect, we have obtained results of violent flame folding linked to acoustic instabilities similar to those reported in [29, 30], for channels with $D/\delta_T = 80$ and $L/\delta_T = 3200$ only when the symmetry of the flame is imposed in the calculation.

It should be noted that even if when symmetric and non-symmetric flames coexist the former are usually mathematically unstable (the real part of the attenuation / growth rate is positive), symmetric solutions may be observed as quasi-stable during experiments. The transition time to stable non-symmetric states depends on the degree of asymmetry in the initial conditions, which are difficult to control in experiments. Accordingly, the flame response to acoustic disturbances can be significantly different in succesive repetitions of the same experiment conducted in a channel of finite length.

Finallly we must mention that in our recent work [19] we have conducted investigations on the effect of differential diffusion and thermal losses to the wall in the flame shape and the breaking of symmetry, showing that heat losses could increase the range stability of symmetric flames while differential diffusion effects would reduce it. Continuing work is now under way, in which we shall investigate the effect of heat losses to the wall and $Le < 1$ in the flame-acoustics interaction.

10. Acknowledgments

This work was financed by projects #PID2019-108592RB-C42 / AEI / 10.13039/501100011033 and #ENE2015-65852-C2-2-R (MINECO/FEDER). The authors thankfully acknowledge the computer resources at MARENOSTRUM and CIBELES and technical support provided by Barcelona Supercomputing Center and UAM (RES-FI-2019-1-0042, IM-2019-2-0006, IM-2020-1-0009 and IM-2020-2-0027).

AppendixA. Resolution tests

We present in this appendix resolution tests for the flame propagating in a channel with $D/\delta_T = 40$ and $L/\delta_T = 800$. To reduce the computational cost, the tests consist in restarting the computation done in the base grid (2000×100) at a time $t\, S_L/L = 0.225$ over a coarsened or a refined grid (using linear interpolation). We compare in Fig. A.17 the pressure measured at the end wall p_w/p_a in the simulations using different mesh resolutions, namely, a coarse 1000×50 grid, the base 2000×100 grid and two refined grids with twice and four times the resolution of the base case simulation. This comparison shows that the measured pressure is similar in the four simulations. However, it is found that the coarser mesh (1000×50: black solid curve) is insufficient at some point, the corresponding simulation can not continue (blows-off) after a time about $t S_L/L = 0.44$ and the flame never reaches the end wall.

We also measured the time t_w taken by the flame to travel from the initial position to the end wall in the simulations using grids with 2000×100, 4000×200 and 8000×400 points and the corresponding average flame speed $\overline{U}$ and present them in table A.1. This table shows that differences between these values as the base case grid is halved are very small and that convergence of the solution is good. We estimated the order of convergence of our simulations by assuming a dependence of the measured quantities t_w and $\overline{U}$ on the grid size as $f(h) = f_0 + A\,(h/\delta_T)^{\alpha}$, with f_0 and A constants, and found $\alpha \approx 1.15$. Note that for t_w the constants are $f_0 = 0.3120$ and $A = 0.104$, respectively, which means that the deviation in the prediction of t_w with the 2000×100 grid is about 1.1%, a very small deviation.

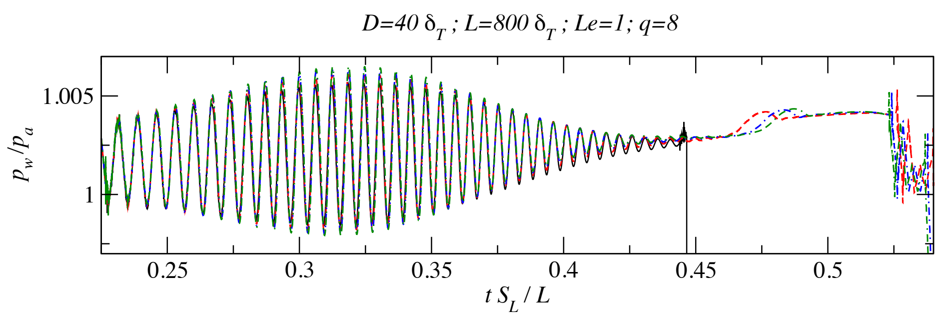

Figure A.17: Pressure oscillations for a flame propagating in a channel with $D/\delta_T = 40$ and $L/\delta_T = 800$ for different resolutions. Solid black line: 1000×50; dashed red line: 2000×100; dashed-dotted blue line: 4000×200; dashed-dashed-dotted green line: 8000×400.

N_x x N_y	h/δ_T	t_w	Δt_w	$\overline{U}$	$\Delta\overline{U}$
2000×100	**0.4**	**0.3156**	-	**1.7229**	-
4000 × 200	0.2	0.3136	-0.0020	1.7341	0.0112
8000 × 400	0.1	0.3127	-0.0009	1.7394	0.0053

Table A.1: Resolution tests in a channel with $D/\delta_T = 40$ and $L/\delta_T = 800$. The base case grid is emphasized.

References

[1] A. C. Fernández-Pello, Micropower generation using combustion: issues and approaches, Proc. Combust. Inst. 29 (2002) 883–899.

[2] D. Dunn-Rankin, E. Leal, D. Walther, Personal power systems, Prog. Energ. Combust. Sci. 31 (2005) 422–465.

[3] Y. Ju, K. Maruta, Microscale combustion: Technology development and fundamental research, Prog. Energ. Combust. Sci. 37 (2011) 669–715.

[4] D. Walther, J. Ahn, Advances and challenges in the development of power-generation systems at small scales, Prog. Energ. Combust. Sci. 37 (2011) 583–610.

[5] K. Maruta, Micro and mesoscale combustion, Proc. Comb. Inst. 33 (2011) 125–150.

[6] N. K. Kaisare, D. G. Vlachos, A review on microcombustion: Fundamentals, devices and applications, Prog. Energ. Combust. Sci. 38 (2012) 321–359.

[7] S. T. Lee, J. S. Tien, A numerical analysis of flame flashback in a premixed laminar system, Combust. Flame 48 (1982) 273–285.

[8] S. T. Lee, C. H. Tsai, Numerical investigation of steady laminar flame propagation in a circular tube, Combust. Flame 99 (1994) 484–490.

[9] J. Daou, M. Matalon, Flame propagation in Poiseuille flow under adiabatic conditions, Combust. Flame 124 (2001) 337–349.

[10] V. N. Kurdyumov, E. Fernández-Tarrazo, Lewis number effect on the propagation of premixed laminar flames in narrow open ducts, Combust. Flame 128 (2002) 382–394.

[11] V. N. Kurdyumov, J. M.Truffaut, J. Quinard, A. Wangher, G. Searby, Oscillations of premixed flames in turbes near the flashback conditions, Combust. Sci. Technol. 180 (2008) 731–742.

[12] V. N. Kurdyumov, Lewis number effect on the propagation of premixed flames in narrow adiabatic channels: Symmetric and non-symmetric flames and their linear stability analysis, Combust. Flame 158 (2011) 1307–1317.

[13] V. Kurdyumov, C. Jiménez, Propagation of symmetric and non-symmetric premixed flames in narrow channels: influence of conductive heat-losses, Combust. Flame 161 (2014) 927–936.

[14] M. Sánchez-Sanz, D. Fernández-Galisteo, V. Kurdyumov, Effect of the equivalence ratio, Damköhler number, Lewis number and heat release on the stability of laminar premixed flames in microchannels, Combust. Flame 161 (2014) 1282–1293.

[15] D. Fernández-Galisteo, C. Jiménez, M. Sánchez-Sanz, V. Kurdyumov, The differential diffusion effect of the intermediate species on the stability of premixed flames propagating in microchannels, Combust. Theory Model. 18 (2014) 582–605.

[16] C. Jiménez, D. Fernández-Galisteo, V. Kurdyumov, DNS study of the propagation and flashback conditions of lean hydrogen-air flames in nar-

row channels: Symmetric and non-symmetric solutions, Int. J. Hydrogen Energy 40 (2015) 12541–12549.

[17] C. Jiménez, V. Kurdyumov, Propagation of symmetric and non-symmetric lean hydrogen-air flames in narrow channels: Influence of heat losses., Proc. Combust. Inst. 36 (2017) 1559–1567.

[18] A. Dejoan, V. Kurdyumov, Thermal expansion effect on the propagation of premixed flames in narrow channels of circular cross-section: Multiplicity of solutions, axisymmetry and non-axisymmetry., Proc. Combust. Inst. 37 (2019) 1927–1935.

[19] A. Dejoan, C. Jiménez, V. Kurdyumov, Critical conditions for non-symmetric flame propagation in narrow channels: influence of the flow rate, the thermal expansion, the Lewis number and heat-losses, Combust. Flame 209 (2019) 430–440.

[20] W. Kaskan, An investigation of vibrating flames, 4th Symposium on Combustion 4 (1953) 575–591.

[21] G. Searby, Acoustic instability in premixed flames, Combust. Sci. Technol. 81 (1992) 221–231.

[22] R. Aldredge, N. Killingsworth, Experimental evaluation of markstein number influence on thermoacoustic instability, Combust. Flame 137 (2004) 178–197.

[23] J. Yáñez, M. Kuznetsov, Flame instabilities of lean hydrogen-air mixtures in a smooth open-ended vertical channel, Combust. Flame 162 (2013) 2830–2839.

[24] F. Veiga-López, D. Martínez-Ruiz, E. Fernández-Tarrazo, M. Sánchez-Sanz, Experimental analysis of oscillatory premixed flames in a hele-shaw cell propagating towards a closed end, Combust. Flame 201 (2019) 1–11.

[25] F. Veiga-López, D. Martínez-Ruiz, M. Kuznetsov, M. Sánchez-Sanz, Thermoacoustic analysis of lean premixed hydrogen flames in narrow vertical channels, Fuel 278 (2020) 118212.

[26] G. Searby, D. Rochwerger, A parametric-acoustic instability in premixed flames, J. Fluid Mech. 231 (1991) 529–543.

[27] P. Pelcé, D. Rochwerger, Vibratory instability of cellular flames propagating in tubes, J. Fluid Mech. 239 (1992) 293–307.

[28] F. Higuera, Acoustic response of a lean premixed flame propagating upward in a tube, Combust. Flame 199 (2019) 377–386.

[29] A. Petchenko, V. Bychkov, V. Akkerman, L. Eriksson, Flame-sound interaction in tubes with no-slip walls, Combust. Flame 149 (2007) 418–434.

[30] A. Petchenko, V. Bychkov, V. Akkerman, L. Eriksson, Violent folding of a flame front in a flame-acoustic resonance, Combust. Flame 145 (2007) 675–687.

[31] C. H. Tsai, The asymmetric behavior of steady laminar flame propagation in ducts, Combust. Sci. Technol. 180 (2008) 533–545.

[32] T. Poinsot, D. Veynante, Theoretical and Numerical Combustion, volume Available at www.cerfacs.fr/elearning, 3d. edition ed., 2012.

[33] T. Poinsot, S. Lele, Boundary conditions for direct simulations of compressible reacting flows, J. Comp. Physics 101 (1992) 104–129.

[34] A. Ghani, T. Poinsot, L. Gicquel, G.Staffelbach, LES of longitudinal and transverse self-excited combustion instabilities in a bluff-body stabilized turbulent premixed flame, Combust. Flame 162 (2015) 4075–4083.

[35] T. Kaiser, G. Öztarlik, L. Selle, T. Poinsot, Impact of symmetry breaking on the flame transfer function of a laminar premixed flame, Proc. Combust. Inst. 37 (2019) 1953–1960.

[36] T. Schuller, T. Poinsot, S. Candel, Dynamics and control of premixed combustion systems based on flame transfer and describing functions, J. Fluid Mech. 894 (2020) P1.

[37] T. Poinsot, D. Veynante, S. Candel, Quenching processes and premixed turbulent combustion diagrams, J. Fluid Mech. 228 (1991) 561606.

[38] T. Poinsot, D. Haworth, G.Bruneaux, Direct simulation and modeling of flame-wall interaction for premixed turbulent combustion, Combust. Flame 95 (1993) 118–132.

[39] B. Cuenot, T. Poinsot, Asymptotic and numerical study of diffusion flames with variable lewis number and finite rate chemistry, Combust. Flame 104 (1996) 111–137.

[40] S. Lele, Compact finite difference schemes with spectral like resolution, J. Comp. Physics 103 (1992) 16–42.

[41] H. Schmidt, C. Jiménez, Numerical study of the direct pressure effect of acoustic waves in planar premixed flames, Combust. Flame 157 (2010) 1610–1619.

[42] C. Jiménez, J. Quinard, J. Graña-Otero, H. Schmidt, G. Searby, Unsteady response of hydrogen and methane flames to pressure waves, Combust. Flame 159 (2012) 1894–.1908.

[43] P. Clavin, P. Pelcé, L. He, One dimensional vibratory instability of planar flames propagating in tubes, J. Fluid Mech. 216 (1990) 299–322.

[44] A. Kaufmann, F. Nicoud, T. Poinsot, Flow forcing techniques for numerical simulation of combustion instabilities, Combust. Flame 131 (2002) 371–385.